TUNNELLING IN NEGATIVE FACE LOSS ENVIRONMENT – FROM RISK TO OPPORTUNITY

Chee Min Khoo[1*], Hisham Mohamad[2]

Abstract

In conventional tunnelling scenario, the face pressure exerted by the Tunnel Boring Machine (TBM) is typically lower than the mobilised earth pressure, resulting in controlled ground movement towards the tunnel face, known as positive face loss. However, negative face loss poses a distinct challenge where the face pressure exceeds the mobilised earth pressure, causing the ground to move away from the tunnel face. This paper presents a full-scale field investigation on tunnel-soil-pile interaction under negative face loss tunnelling environments. The study integrates field measurements with numerical analysis to assess the transient effects of shield tunnelling on a fully instrumented experiment pile, which was pre-loaded and equipped with strain gauges, an inclinometer, and distributed fibre optic sensing. Real-time monitoring was conducted throughout the tunnel advancement, while three-dimensional finite element modelling was developed using actual TBM driving data to simulate pile responses as various tunnelling stages. The field observations and numerical results validate the hypothesised movement paths of the pile under negative face loss and offer new insights into the pile's behaviour. The study highlights the importance of controlling tunnel volume loss, with an optimal TBM face pressure range recommended between 0.8 and 1.1 times the overburden pressure, and grouting pressure between 1.1 and 1.5 times the overburden pressure to mitigate ground settlement. The validated numerical framework serves as a basis for further parametric studies and provides practical recommendations for risk mitigation and enhanced tunnelling efficiency. These findings mark a significant advancement in understanding tunnelling-induced effects on piles, transforming negative face loss from a mere risk into a potential opportunity for optimised tunnelling performance.

Received: *21 January, 2025*
Revised: *3 March, 2025*
Accepted: *15 April, 2025*

[1,2]Department of Civil and Environmental Engineering, Universiti Teknologi PETRONAS, 32610 Seri Iskandar, Perak, Malaysia.

****Corresponding author:***
khoocheemin@gmail.com

DOI: *https://10.54552/v86i2.272*

Keywords:
Tunnel-soil-pile interaction, Tunnelling-induced pile responses, Transient effects, Negative face loss, Distributed fibre optic sensing

List of Notations

y is the distance between the TBM face and the experiment pile
D is the tunnel diameter
p_f is the face pressure
p_g is the tail skin grouting pressure
σ is the overburden pressure

1.0 INTRODUCTION

Shield tunnelling using pressurised face Tunnel Boring Machines (TBMs), such as Earth Pressure Balance (EPB) and slurry shields, is a highly mechanised, relatively safe, and fast tunnel construction method. In a typical tunnelling scenario, the face pressure exerted by the TBM remains lower than the mobilised earth pressure, allowing for controlled advancement as the ground moves towards the machine. This phenomenon generally results in predictable surface settlement, consistent with the principle of positive face loss. In contrast, negative face loss presents a unique challenge. Here, the face pressure exceeds the mobilised earth pressure, pushing the ground away from the TBM face and potentially causing surface heave. This can pose risks to underground utilities, above-ground structures, and the environment if not managed effectively.

In the case of a tunnelling adjacent to a pile foundation, where the pile is initially in equilibrium with long-term external loads and soil consolidation before tunnel excavation, the excavation disrupts this balance, causing additional deformation and stress adjustments in both the surrounding soil mass and the pile foundation. Due to the redistribution of deformation and stress induced by tunnel excavation, the pile experiences displacements in various directions based on its location relative to the TBM and the magnitude of ground loss components, such as face loss, shield loss, and tail loss (Loganathan, 2016). In the context of negative face loss condition, the pile moves outward as the TBM approaches. After the TBM passes, positive shield and tail loss occurs, causing the pile to move toward the tunnel. Figure 1 depicts the pile movement path in this scenario. Therefore, understanding the dynamics of TBM operating pressures and volume loss is crucial for tunnelling projects, as it governs ground behaviour and pile movement patterns. Both the capacity and serviceability of the piles in response to tunnelling-induced transient effects must be carefully evaluated.

Considerable research has been conducted on tunnelling beneath or adjacent to piles, employing various methodologies including field studies, laboratory centrifuge tests, and empirical, analytical, and numerical approaches. However, most of these studies focus on frictional or frictional-end bearing piles, with the exception of a socketed pile modelled in one of the centrifuge

tests by Ong (2009). In full-scale field studies, pile responses to nearby tunnelling have often been evaluated indirectly through monitoring of structures and ground instrumentation. Direct in-pile instrumentation, however, has been limited, presenting opportunities for more in-depth investigations. Some notable in-pile instrumentation field studies are summarised in Table 1, where the instrumented piles had their toe levels terminated either above the tunnel crown or beside the tunnel extrados at varying depths.

Results from in-pile instrumentation revealed distinct zones of influence around tunnels during construction. Within these zones, both the ground and piles experienced varying degrees and directions of relative displacements. As the TBM approached, passed beneath or adjacent to, and continued beyond the pile, notable redistributions of load along the pile lengths were observed. This phenomenon induced lateral pile deflections and bending moments, some of which were transient and reversible, depending on the prevalence of several factors (Khoo, 2024). However, few researchers have focused on pile lateral deflection. Loganathan's (2016) hypothesis on the settlement influence zone and pile movement paths remains an area worth exploring.

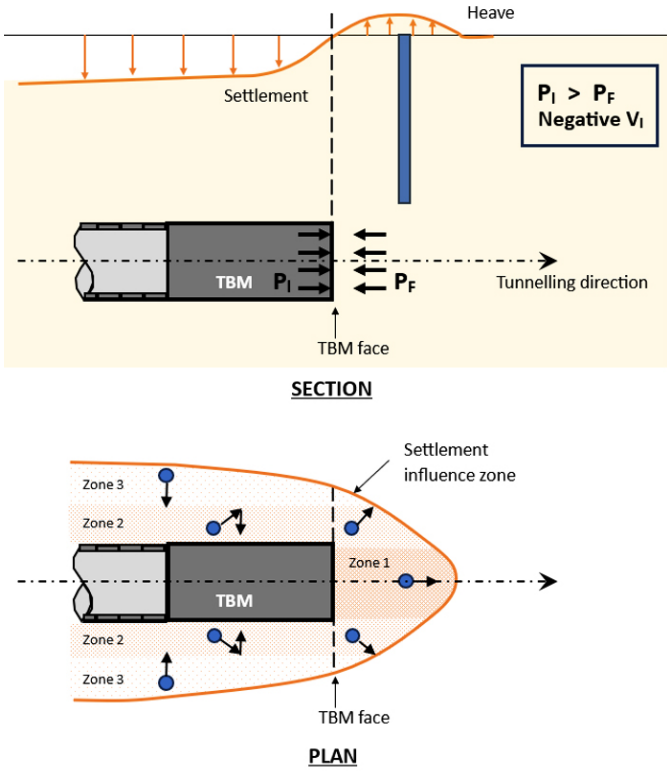

Figure 1: Ground response and pile movement path in negative face loss scenario (Loganathan, 2016)

To contribute to this body of knowledge, full-scale field research was recently conducted at Malaysia's Klang Valley Mass Rapid Transit (KVMRT) - Putrajaya Line. The study builds on previous efforts and addresses gaps in knowledge by employing distributed fibre optic sensing technology based on stimulated Brillouin scattering, using the Brillouin Optical Time Domain Analysis (BOTDA) technique, to monitor real-time strain in a pre-loaded experiment micropile in close proximity to twin bored tunnels excavated using Variable Density (multimode) TBMs. This novel technique offers several advantages over conventional point-based sensors (e.g. strain gauges) for assessing tunnel-soil-pile interactions (Soga *et al.,* 2008). It is also effective in identifying anomalies in cast-in-situ concrete piles (Mohamad *et al.,* 2016). The integrated sensors measure three-dimensional deformations, including bending and lateral displacements, providing more precise data on tunnel-soil-pile interaction and pile responses throughout the entire pile length during the transient effects of shield tunnelling. This advanced technology has proven effective in monitoring various large civil and geotechnical structures, including piles (Ohno *et al.,*2002, Klar *et al.,* 2006), test piles (Mohamad *et al,* 2009; Tee *et al.,* 2016; Tee *et al.,* 2017), retaining walls (Mohamad *et al.,* 2011), as well as bridges and tunnels (Mohamad *et al.,* 2010; Mohamad *et al.,* 2012).

Field data from the research site were interpreted and back-analysed using three-dimensional finite element modelling, alongside TBM driving data recorded during tunnelling. Numerical results from the tunnel-soil-pile interaction analysis were validated with field measurements. The validated framework has opened avenues for further exploration through numerical parametric studies. This paper aims to deepen the understanding of the transient effects of shield tunnelling on a loaded pile in a negative face loss environment, offering valuable insights for the scientific and tunnelling community, along with recommendations and strategies to mitigate risks

Table 1: Summary of reported field studies with in-pile instrumentation

Citation	Project	Soil Type	Tunnel Type	Pile Type	In-Pile Monitoring
Mair (1993) Lee *et al.* (1994)	Angel Underground Station, London	London clay	Hand-dug tunnel	Bored pile (under-reamed)	Inclinometer
Teunissen & Hutteman (1998) Kaalberg *et al.* (2005)	North/South Line, Amsterdam	Very soft silty clay overlying sand layer	Shield tunnel	Timber pile, concrete pile	Pile top pressure sensor, precise levelling
Coutts & Wong (2000) Pang *et al.* (2005)	North-East Line C704, Singapore	Bukit Timah granitic residual soil	EPB shield tunnel	Bored pile	Vibrating wire strain gauge
Jacobsz *et al.* (2005) Selematas *et al.* (2005)	Channel Tunnel Rail Link C250, Essex, UK	Terrace gravel and London clay	EPB shield tunnel	Driven pile, bored pile	Vibrating wire strain gauge, base load cell, electrolevel inclinometer
Cham (2007)	Circle Line C852, Singapore	Bukit Timah granitic residual soil	EPB shield tunnel	Bored pile	Vibrating wire strain gauge
Mohamad *et al.* (2022)	Grand Paris Express Line 16, France	Fine clayey sand overlying limestone	EPB shield tunnel	Cast-in-situ pile	Strain gauge, optical fibre cable

associated with pile responses during various stages of tunnel excavation. The findings underscore the delicate balance in negative face loss tunnelling, where careful management can mitigate risks while enhancing tunnelling safety and efficiency.

2.0 BACKGROUND OF THE STUDY

2.1 The Research Site

The research site is located at the Education Quarters in the central business district of Kuala Lumpur and was designated for a full-scale field investigation. This is part of the KVMRT Putrajaya Line project, where twin bored tunnels, each with a diameter of 6.35 m, were driven partially beneath the Quarters. The tunnelling commenced from the northwest at Hospital Kuala Lumpur (HKL) Cross-over and extended southeastward to Raja Uda Station, as illustrated in Figure 2. Notably, the southbound tunnel passed directly beneath a 5-storey building, presenting significant challenges due to the presence of the existing building foundations.

To mitigate this challenge, the affected piles were removed, and underpinning work was carried out ahead of the TBM passage. The underpinning process involved the installation of micropiles capped under a reinforced concrete transfer structure, which spanned across the tunnel. Given the anticipated complexities of the tunnel construction, an additional 'experiment' micropile was strategically installed. Figure 3 provides a plan view and cross-section of the tunnel relative to the existing building foundation, newly installed underpinning

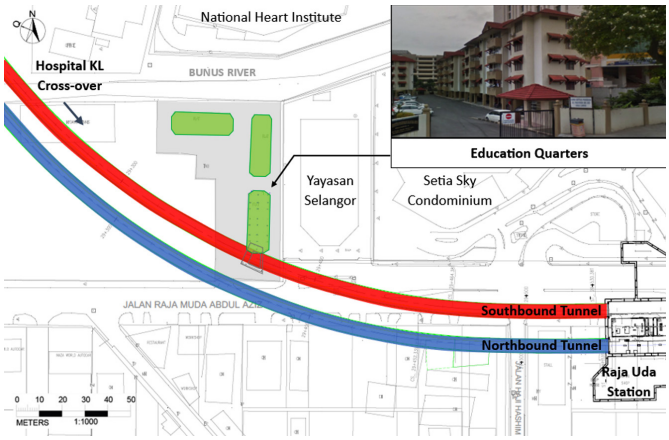

Figure 2: Location plan of the research site

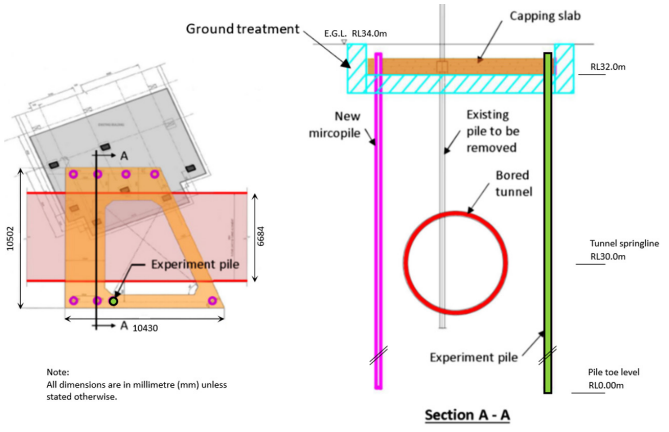

Figure 3: Plan view and cross-section of the underpinning works

piles, and the experiment pile. Detailed information of the pile removal and underpinning works can be found in the references (Tan *et al.,* 2019, Khoo *et al.,* 2024a). This strategic decision enabled comprehensive in-pile instrumentation and real-time monitoring throughout the tunnelling process, with the experiment pile playing a critical role in providing insights into the interactions and transient responses of the pile-tunnel system.

2.2 Ground Characterisation

The site is located within the Kuala Lumpur Limestone formation, characterised by flat terrain with an average elevation of Reduced Level (RL) 34 m. Site investigations confirmed the expected regional geological setting, revealing alluvium overlying limestone bedrock. However, the bedrock levels at the site were predicted to be erratic, with potential cavities due to the karstic features inherent in the limestone formation. The alluvium consists mainly of interbedded layers of loose sand and soft clay/silt. Groundwater was encountered at a depth of 4 m at the research site, with a typical seasonal fluctuation of ±0.5 m. Figure 4 illustrates the interpreted geological profile along the southbound tunnel alignment, where the tunnel is located, with cover-to-diameter ratios ranging from approximately 1.6 to 2.0.

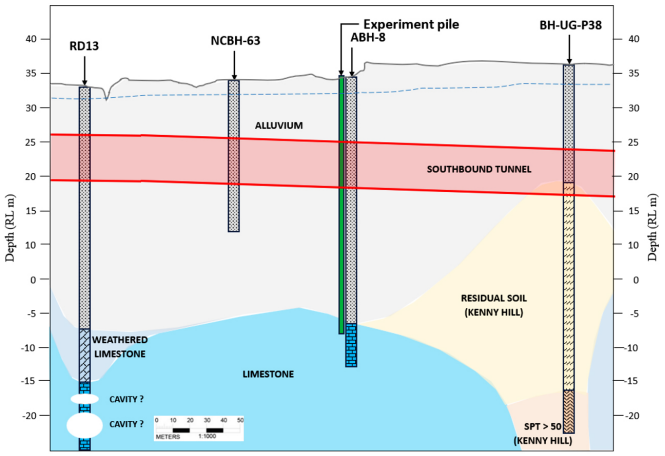

Figure 4: Interpreted geological profile along the southbound tunnel alignment

The ground stratification consists of alluvium overlying limestone bedrock, and the pile, being socketed int the bedrock, provides a controlled environment with a fixed-end condition. This feature represents a novel aspect to the research, as, to the best of the authors' knowledge, no prior studies have specifically investigated this scenario.

2.3 The Experiment Pile and Instrumentation

The experiment pile, with a diameter of 300 mm, was positioned 1.5 m away from the extrados of the southbound tunnel. It is reinforced with an API (American Petroleum Institute) pipe, measuring 177.8 mm in outer diameter and 10.36 mm in wall thickness. The pile was installed to a depth of 1.5 m into the limestone bedrock at 32.3 m below ground level. The micropile (Grade G30) is designed with a working capacity of 600 kN. Key details of the experiment pile are summarised in Table 2. A detailed account on the pile head setup for pre-loading can be found in Khoo *et al.* (2024a).

Table 2: Details of the experiment pile

Parameter	Unit	Value
Pile diameter	mm	300
Pile working load	kN	600
Pile reinforcement	-	API pipe (177.8 mm O.D. with 10.36 mm wall thickness)
Cement grout grade	MN/m^2	30
Water cement ratio	-	0.45 . 1.00
Rock socket length	m	1.5
Total pile length	m	33.8
Date of installation	-	16 March 2018

The in-pile instrumentation was meticulously designed to provide real-time data on the tunnelling-induced transient pile responses, including vertical displacement at the pile head, horizontal deformation of the pile shaft, axial load distribution, and internal forces within the pile. This instrumentation incorporated both conventional vibrating wire strain gauges and inclinometer, as well as advanced fiber optic distributed sensors. The integration of both conventional and advanced sensing technologies enhances the reliability and accuracy of measurements, enabling a comprehensive evaluation of the pile's response to tunnelling-induced transient effects. Details of the in-pile instrumentation and arrangement are illustrated in Figure 5.

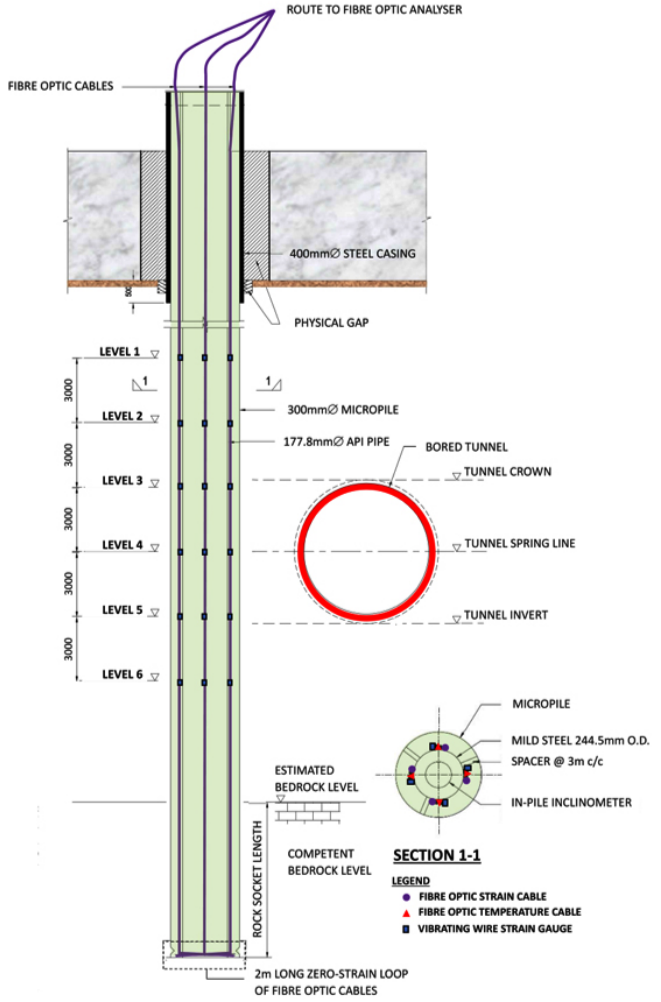

Figure 5: In-pile instrumentation and arrangement

Six levels of vibrating wire strain gauges were strategically affixed to the pile reinforcement (API pipe). These gauges were placed at 3-meter intervals, beginning from a depth of 4 m below the ground surface. Each level corresponds to significant measuring points. Level 1 – 6 m above the tunnel crown, Level 2 – 3 m above the tunnel crown, Level 3 – tunnel crown, Level 4, tunnel springline, Level 5 – tunnel invert, and Level 6 – 3 m below tunnel invert. At every level, the strain gauges were arranged on four sides (two pairs per level), with each pair aligned parallel and perpendicular to the tunnel orientation. These strain gauges were spot-welded on 10 mm steel bands and securely fastened to the designated levels on the API pipe. Unfortunately, some sensors did not survive the installation process.

Additionally, an inclinometer casing was pre-installed inside the API pile during the grouting process, providing redundancy for pile deflection measurements and ensuring comprehensive data collection on the pile's behaviour during the tunnelling process. The baseline measurement, which was used for interpretation, was conducted one month before the TBM reached the target, to eliminate any strain induced by the installation process.

In addition to the in-pile instrumentation, settlement markers, inclinometers, and piezometers were installed in the ground adjacent to the experiment pile. The building that the tunnel undercrossed was also closely monitored. This comprehensive instrumentation regime enabled a thorough investigation of tunnelling-induced effects and tunnel-soil-pile interaction. Figure 6 illustrates the ground and structure instrumentation surrounding the experiment pile.

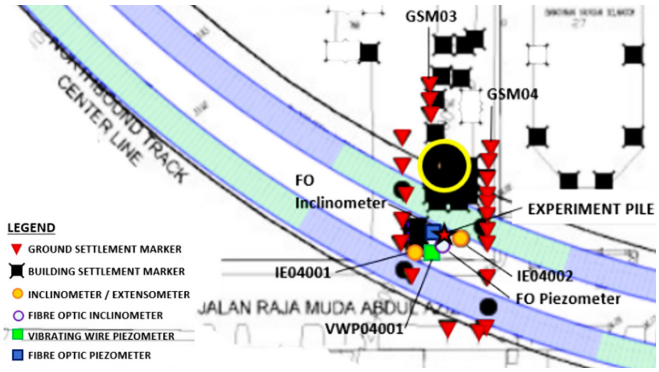

Figure 6: Ground and structure instrumentation

3.0 FIELD MEASUREMENTS AND NUMERICAL ANALYSIS

3.1 Key Tunnelling Data

The installation of the instrumented experiment pile was completed in March 2018, followed by pile removal work ahead of the passage of the TBMs. Construction activities were carefully coordinated to ensure that the underpinning and pile removal did not interfere with tunnelling operations or affect the permanent tunnel lining. Consolidation due to the piling and ground treatment works was assumed to be complete prior to TBM advancement, given the high permeability of the alluvium sandy soil.

This study specifically focused on the southbound tunnelling over a distance of approximately between y = -10D and +10D from the experiment pile, as illustrated by the time-location of

the TBM in Figure 7, where y represents the distance between the TBM face and the experiment pile, normalised by the tunnel diameter (D). Positive values of y indicate distance where the TBM has passed beyond the pile. This section of tunnel was completed between 3 May 2019 and 16 May 2019. It is important to note that the TBM stopped for planned cutterhead intervention on 6 and 7 May 2019, which took place within a grout block.

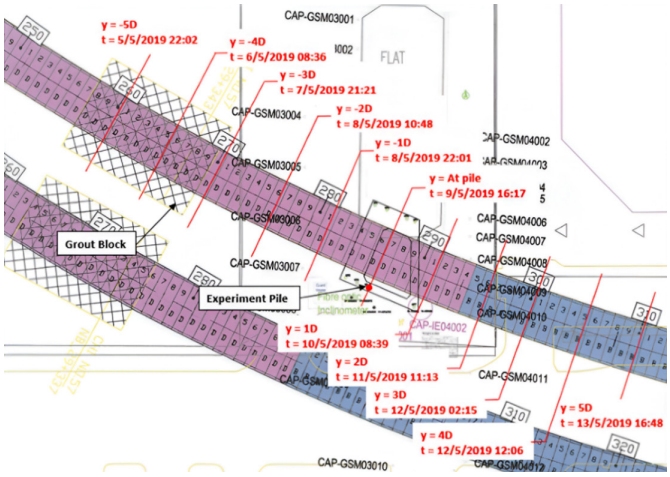

Figure 7: Time-location of the southbound TBM in relation to the experiment pile

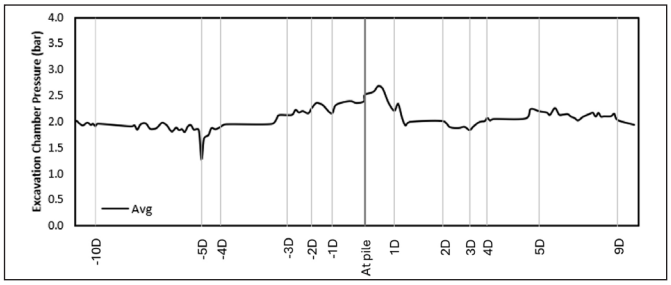

Figure 8: Recorded excavation chamber pressures

Variable density tunnel boring machines were selected for excavating the tunnels from HKL Cross-over to Raja Uda Station, operating in the earth pressure balance (EPB) mode. During the TBM progress, a continuous range of face support pressure was provided. Figure 8 shows the recorded average face pressure in the excavation chamber. It is evident that a higher face pressure was applied ahead of the experiment pile. The face pressure gradually increased from 2 bar (at a distance of y = -3D) to a maximum of 2.6 bar as the TBM cutterhead reached the experiment pile location, eventually decreasing to the normal face pressure at a distance of 1D away.

As part of the key tunnelling data, the normal range of advance speed was between 20 – 50 mm/min, with an average of 34.5 mm/min for this length of the bored section. Advance thrust forces and group pressures fluctuated between 10 – 17 MN and 50 – 150 bar, respectively. The grouting pressure at the grout ports remained relatively constant throughout the tunnel drive, with average pressures approximately 2 - 4 bar.

3.2 Numerical Simulation

The three-dimensional numerical modelling and simulation were conducted using a commercially available finite element program, PLAXIS 3D, to replicate tunnel advancement in a manner closely resembling actual excavation processes. A comprehensive 3D model with dimensions of 140m in length, 40 m in height, and 100 m in width was employed for the analysis, consisting of 56,584 elements and 88,440 nodes, as shown in Figure 9. Readers are referred to Khoo *et al.* (2024b, 2025) for further details on the model set-up, soil constitutive model, and material properties. This paper reiterates some of the key simulation techniques adopted.

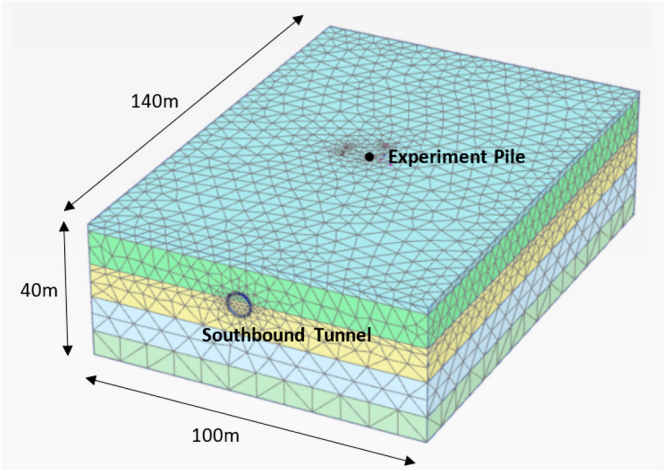

Figure 9: Perspective view of the developed 3D model

The model simulated the first 42 m of tunnels modelled using the "all-in-once installation" approach (Vermeer *et al.,* 2002), followed by a step-by-step simulation to represent sequential tunnel advancement. The recorded face pressures from the TBM excavation chamber were applied to the tunnel face using a multi-segmental trapezoidal profile instead of the conventional triangular earth pressure (Khoo *et al.,* 2024b). This approach accounted for pressure loss along the screw conveyor in EPB tunnelling, where the pressure gradually decreases, and reaching zero at the discharging outlet. According to Herrenknecht & Rehm (2003), as reproduced in Figure 10, the pressure at the screw conveyor inlet reduces to 80% of the applied face pressure, with the pressure gradient influenced by the fluidity and impermeability of the muck. The irregular pressure distribution reflects the inherent challenges in maintaining a classical earth pressure profile during excavation.

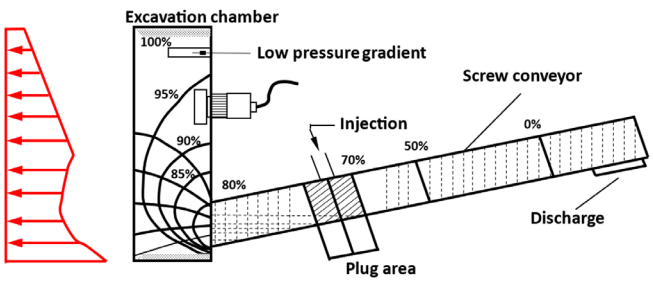

Figure 10: Earth pressure distribution diagram (Herrenknecht and Rehm, 2003)

As shown in Figure 11, tail void grouting was modelled by applying radially distribution isotropic pressure around the tunnel periphery to replicate the injection pressure of grout in its fluid state. This grouting simulation method has been widely adopted by researchers, including Kasper & Meschke (2004)

and Mollon *et al.* (2013). The recorded grouting pressures during tunnel advancement were incorporated into the numerical model to improve the simulation's realism and accuracy.

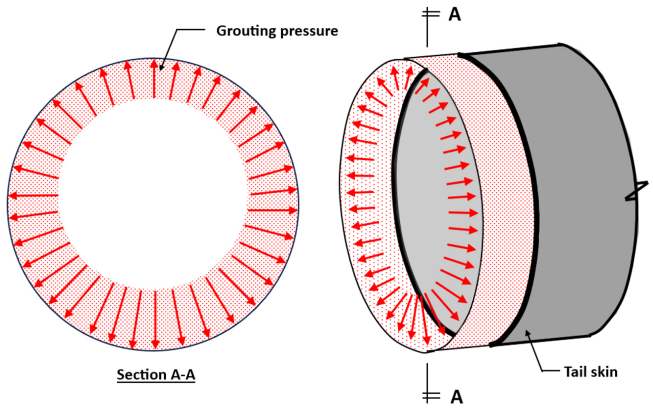

Figure 11: Profile of radial distribution grouting increasing with depth adopted in the simulation

3.3 Field Measurements and Numerical Analysis Results

The initial step in the study involved comprehensive calibration and validation of the numerical model to verify the experiment pile's load-settlement behaviour and axial load distribution during the pre-loading stage, before being subjected to tunnelling effects. The observed agreement (> 95%) between computed and measured pile head settlements (Figure 12), as well as pile load distributions (Figure 13), underscores the validity of the numerical framework established in this study (Khoo, 2024).

The numerical analysis results were subsequently compared with field measurements, focusing on transient pile responses such as pile head movement, axial load distribution, bending moments, and lateral deflection. This comprehensive comparison demonstrates the numerical simulations' accuracy and reliability in capturing the dynamic behaviour of the pile under tunnelling-induced effects. For detailed comparisons of pile head movement, axial load distribution, and bending moments between field measurements and numerical back-analysis, readers are referred to Khoo *et al.* (2025). This paper provides a summary of the key findings related to pile lateral deflection.

Figure 14 presents a detailed view of the time-based movement path of the pile at six critical depths. In this illustration, the positive direction of Axis-A indicates movement away from the tunnel in the transverse direction, while the positive direction of Axis-B denotes movement away from the tunnel face in the longitudinal direction.

Both the field measurements and numerical results consistently demonstrate that as the TBM approached the target, the pile generally experienced outward movement, with the exception of Level 1 in the numerical analysis. This anomaly may be attributed to the numerically simulated top-loaded fixed-end pile behaving as a slender bending element. Once the TBM face passed the pile, the lateral deflection at tunnel level promptly shifted back towards the tunnel as the distance increased, although the numerical analysis indicated slight variations in direction.

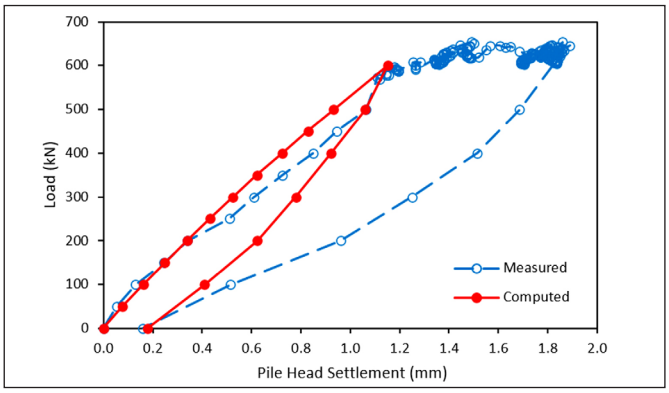

Figure 12: Load settlement behaviour of the experiment pile

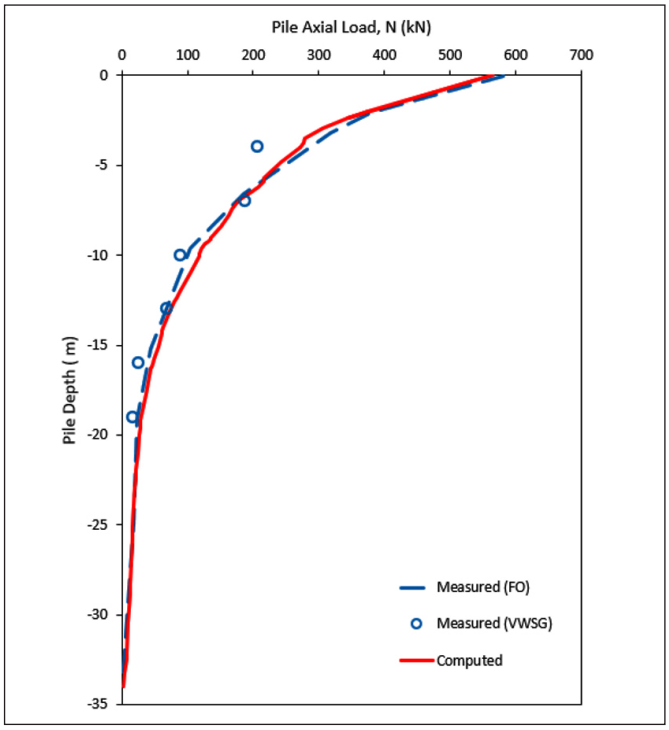

Figure 13: Axial load distribution along the experiment pile

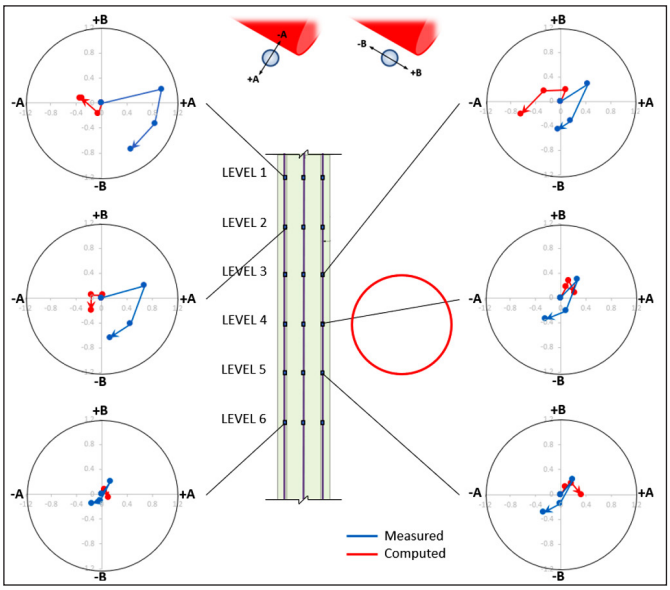

Figure 14: Incremental pile movement during the tunnel advance

These findings align with the hypothesis proposed by Loganathan (2016) regarding pile movement paths in a negative face loss scenario. According to this hypothesis, when the TBM face pressure exceeds the mobilised earth pressure at the face, the ground is pushed away from the TBM face, inducing heave at the surface and sub-surface ground movement away from the TBM face. Subsequently, when the TBM has passed, a positive shield and tail loss occurs, signalling the closing of the physical gap. This results in the ground moving toward the tunnel, leading to ground settlement. This entire phenomenon was evidenced by the measured ground surface movements as depicted in Figure 15. Additionally, the measurement of building settlement, shown in Figure 16, further validates these observations. Refer Figure 6 for the locations of the instrumentation.

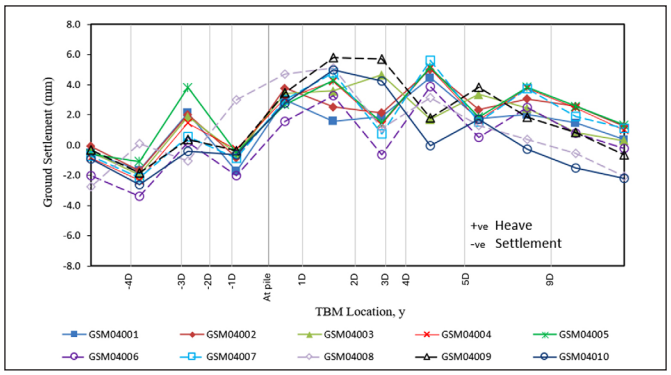

Figure 15: Measured ground surface movements

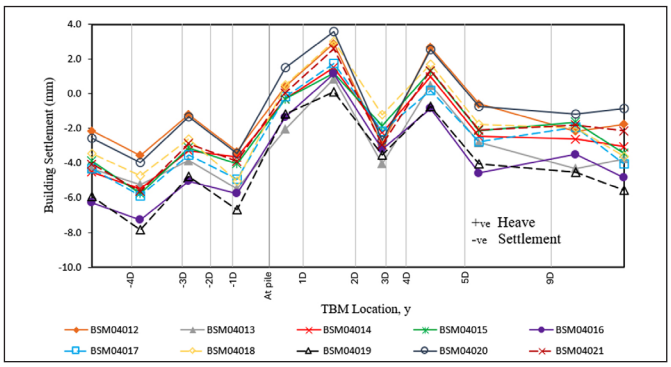

Figure 16: Measured building settlements

4.0 PARAMETRIC STUDY

Following the successful back-analysis and validation of the three-dimensional (3D) finite element model using valuable TBM operating data and field measurements from the research site, a series of parametric studies has been implemented to identify an optimum range of tunnelling parameters for controlling ground loss and minimising the impacts on the adjacent pile during various stages of tunnel excavation. Specifically, the influence of face support pressure and tail skin grouting pressure is assessed, providing insights into the significance of each parameter concerning the pile responses induced by tunnelling.

4.1 Effects of Face Support Pressure

The application of face support pressure is normalised to the overburden pressure (p_f/σ) at the tunnel crown level, with specified variations as outlined in Table 3. These diverse ranges are calibrated to the validated research site data to observe pile responses and the magnitude of ground surface settlement while maintaining consistent soil properties, pile properties, and other TBM driving parameters. The analyses aim to ascertain the relationship between applied face pressure and key effects on pile responses, including pile head displacement, pile lateral deflections (perpendicular and parallel to the tunnel), and pile axial load.

Table 3: Variation of face support pressure

Face Pressure, p_f (kN/m^2)	Ratio to Baseline	p_f/σ
48.75	0.25	0.3
97.50	0.50	0.5
146.50	0.75	0.8
195.00	1.00	1.1
243.75	1.25	1.4
292.50	1.50	1.6
341.25	1.75	1.9
390.00	2.00	2.2

When the normalised face pressure (p_f/σ) exceeds 1.0, a negative face loss scenario occurs. Otherwise, it is considered as positive face loss, where the face pressure is within the range of overburden pressure or significantly lower than the overburden pressure.

For each applied face pressure, the evolution of the impacts is studied for a distance of TBM advance from y = -2D up to y = 9D from the experiment pile, where y is the distance between the TBM face and the experiment pile, normalised by the tunnel diameter (D). The negative distance signifies the TBM's position prior to reaching the pile. This range of distance is selected considering the recommended zone of influence from the research study (Khoo *et al.*, 2025) as well as a sufficiently long distance for stabilising the equilibrium of tunnelling effects.

4.1.1 Pile Head Displacement

Figure 17 illustrates the pile head settlement at various p_f/σ values. Generally, it can be observed that the pile head experiences a lesser magnitude of settlement within the range of p_f/σ between 0.8 and 1.1. This trend is evident as the TBM passes by the pile until a distance of y = 3D. However, there is a noticeable increase in pile head settlement when p_f/σ exceeds 1.1.

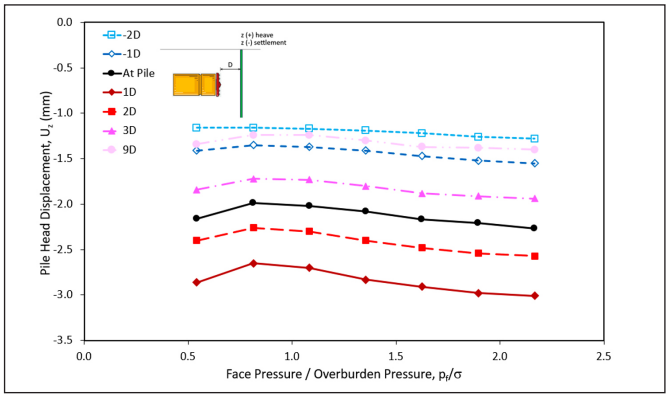

Figure 17: Pile head displacement, U_z vs. face pressure/overburden pressure, p_f/σ

It should be emphasised, however, that the numerical model fails to converge if p_f/σ is less than 0.5. This implies that a minimum face support pressure is required for the successful simulation of this project case study. In practice, if the face support pressure decreases further, significant deformation or total collapse of the soil body may occur.

4.1.2 Pile Lateral Deflections

Figure 18 illustrates the maximum pile lateral deflections at various p_f/σ values for the transverse direction (perpendicular to the tunnel). Positive values indicate movement away from the tunnel extrados. Generally, the pile lateral deflection becomes noticeable in the transverse direction when the p_f/σ ratio is about 1.4 or higher. The same trend is observed for an approaching TBM at y = -1D, with the magnitude of deflection continuously increasing until the TBM has passed far beyond the pile.

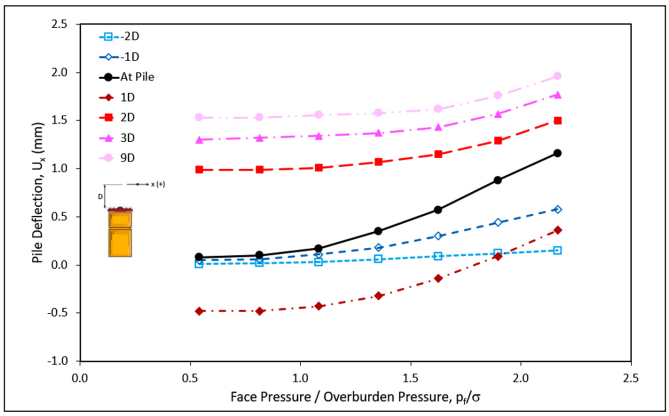

Figure 18: Pile lateral deflection, U_x vs. face pressure/overburden pressure, p_f/σ

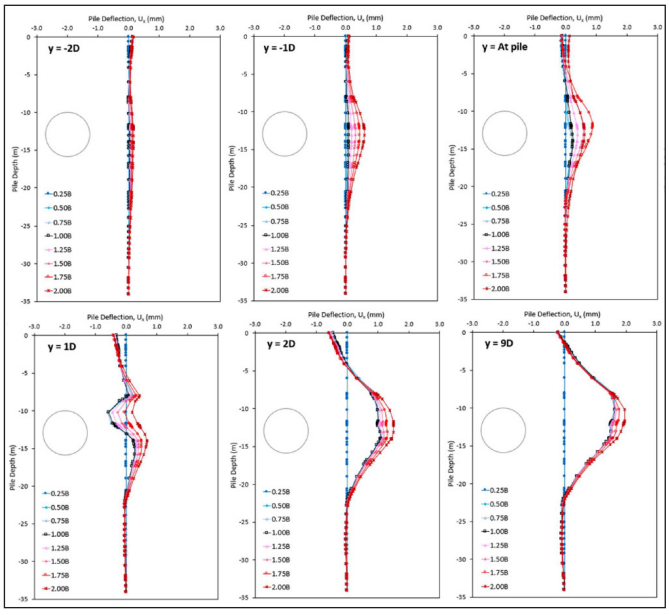

Figure 19: Evolution of pile lateral deflection, U_x profile

The evolution of pile lateral deflection profiles is illustrated in Figure 19. From here, we can see that the pile movement path is obvious, especially for the case of negative face loss ($p_f/\sigma > 1.0$), where the pile is being pushed away when the TBM is approaching and being pulled inward at y = 1D (where the shield is passing through the pile) temporarily before release outward after the entire TBM shield has passed beyond the pile a distance of y = 2D. The maximum pile lateral deflection occurs in a zone above the tunnel springline to the tunnel crown.

Opposite to the transverse direction, the magnitude of pile lateral deflection in the longitudinal direction significantly and linearly increases with the increased p_f/σ ratio, even from a lower ratio of 0.5, as shown in Figure 20. Logically, a higher face pressure applied will directly push the pile forward along the tunnel alignment. The pile lateral deflection reaches its peak when the TBM face approaches the pile and starts to decrease after the TBM passed beyond.

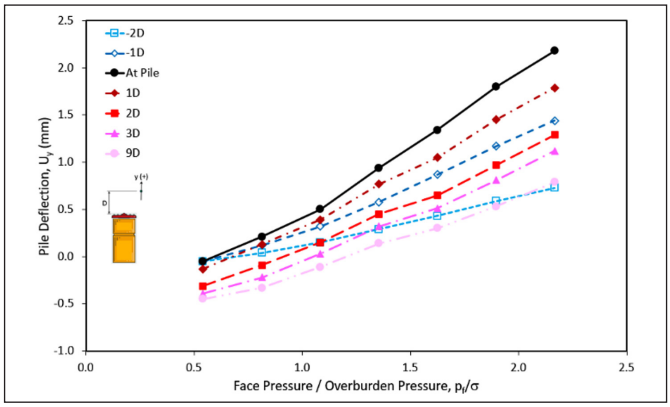

Figure 20: Pile lateral deflection, U_y vs. face pressure/overburden pressure, p_f/σ

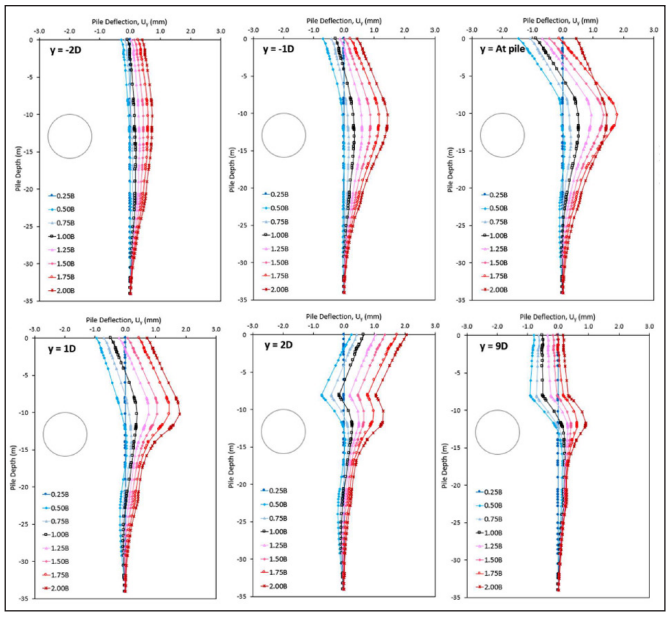

Figure 21: Evolution of pile lateral deflection, U_y

In a similar presentation, Figure 21 illustrates the evolution of pile lateral deflection in the longitudinal direction. Similar pile movement behaviour is noted except that the incurred inward movements are irreversible as observed when TBM passed far beyond the pile, y = 9D. This observation tallies with the hypothesis proposed by Loganathan (2016) for a negative face loss tunnelling environment, where the ground is pushed away from the TBM face, may induce heave at the surface and subsurface ground movement away from the TBM face,

subsequently, when the TBM has passed, a positive shield and tail loss occurs, signifying the closing of the physical gap. This results in the ground movement toward the tunnel, leading to ground settlement.

4.1.3 Pile Axial Load

Regarding the pile axial load, the evaluation focuses on the maximum value occurring in the critical zone between one time diameter above and below the tunnel horizon. This is crucial as the maximum axial load, attributed to the additional drag load due to tunnelling-induced ground settlement, typically occurs at the tunnel horizon.

Figure 22 illustrates the impacts on pile axial load in response to the varying applied face pressure. Despite the pile axial load generally being unresponsive to higher face pressure, a reduced load is obtained when the p_f/σ ratio is around 0.8 to 1.1 as observed when the TBM is at y = 1D, as shown in Figure 22.

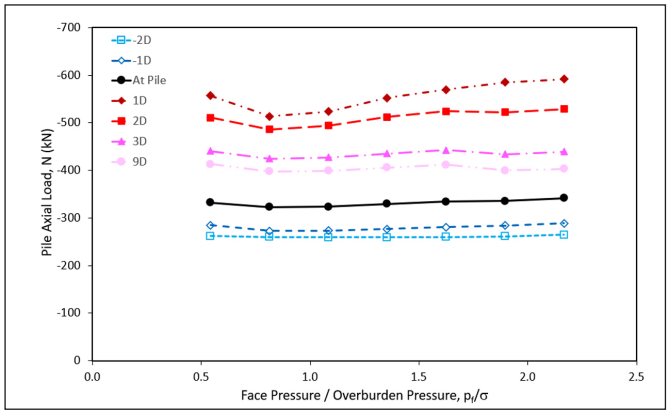

Figure 22: Pile axial force vs. face pressure/overburden pressure, p_f/σ

4.1.4 Ground Surface Settlement

Figure 23 illustrates the general trend of maximum ground settlement and ground loss obtained for the range of p_f/σ ratio adopted in this study. Clearly, the recommended optimum face pressure is between 0.8 to 1.1 times the overburden pressure, aligning with the earlier observations.

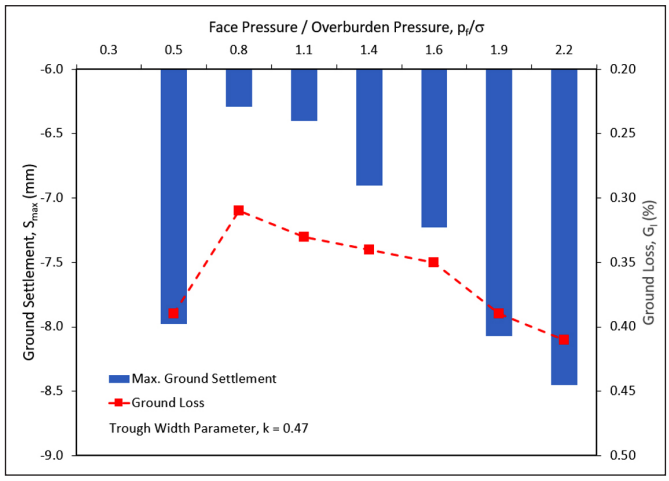

Figure 23: Ground settlement vs. face pressure/overburden pressure, p_f/σ

4.2 Effects of Tail Skin Grouting Pressure

Similar to the face support pressure analyses, this set of studies will vary the normalised grouting pressure to assess its impact on pile responses. The applied pressure will be increased up to three times the overburden pressure to explore potential beneficial effects. The relationship between applied grouting pressure and variables such as pile head displacement, pile lateral deflections, axial load and ground surface settlement will be examined.

In exploring the impact of tail skin grouting, grouting pressure is normalised to the overburden pressure at the tunnel axis level, spanning a specified range (Table 5).

Table 5: Variation of tail skin grouting pressure

Grouting Pressure, p_g (kN/m²)	Ratio to Baseline	p_f/σ
87.5	0.25	0.6
175.5	0.50	1.2
262.5	0.75	1.8
350.0	1.00	2.4
437.5	1.25	3.0
525.0	1.50	3.6
612.5	1.75	4.3
700.0	2.00	4.9

4.2.1 Pile Head Displacement

Figure 24 illustrates the results of pile head settlement at various p_g/σ values. The pile exhibits responsiveness to tail skin grouting effects when the TBM face is at y = 2D, aligning with the shield tail coinciding with the pile position. Generally, pile head settlement diminishes with an increasing p_g/σ ratio, indicating pile rebound. Notably, the pile may experience an upward heave with substantial grouting pressure, particularly when the p_g/σ ratio exceeds 2.0.

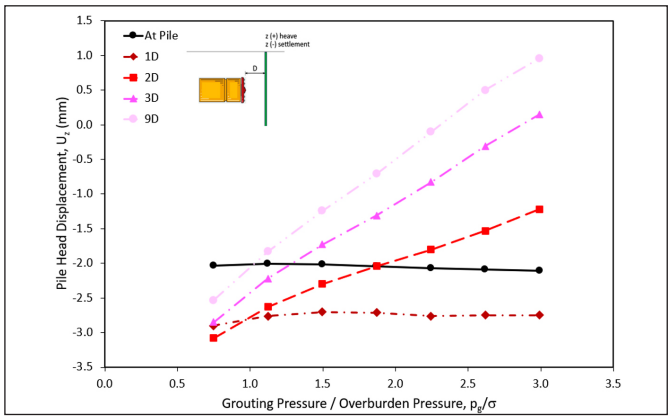

Figure 24: Pile head displacement, U_z vs. grouting pressure/overburden pressure, p_g/σ

It is essential to highlight that the simulation adopted radially distributed pressure around a tunnel ring (perpendicular to the ground), deviating from real-word scenarios where grouting pressure is applied to the annulus gap between the lining and surrounding soil. Additionally, the study observes temporary compression of the pile due to downdrag load generated during TBM passage, with subsequent release after the TBM surpasses y = 3D. The rate of pile rebound consistently heightens as the TBM moves farther away.

Similar to the prior face pressures study, convergence issues arise if p_g/σ is less than 0.5, underscoring the need for a minimum grouting pressure for successful simulation in this project case study.

4.2.2 Pile Lateral Deflection

Figure 25 provides an overview of pile lateral deflections at various p_g/σ values for the transverse direction (perpendicular to the tunnel).

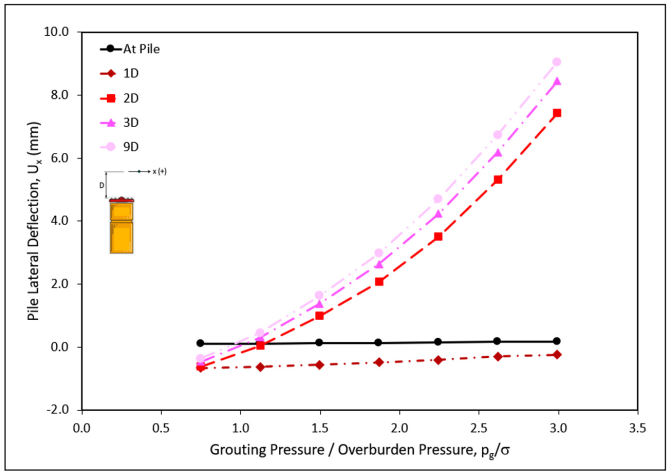

Figure 25: Pile lateral deflection, U_x vs. grouting pressure/overburden pressure, p_g/σ

The behaviour of pile lateral deflection in the transverse direction mirrors that of pile head settlement, given the adoption of radially distributed pressure in simulating tail skin grouting pressure. Notably, lateral deflection exhibits exponential growth with an increasing p_g/σ ratio. Similar patterns are observed in the longitudinal direction, as depicted in Figure 26.

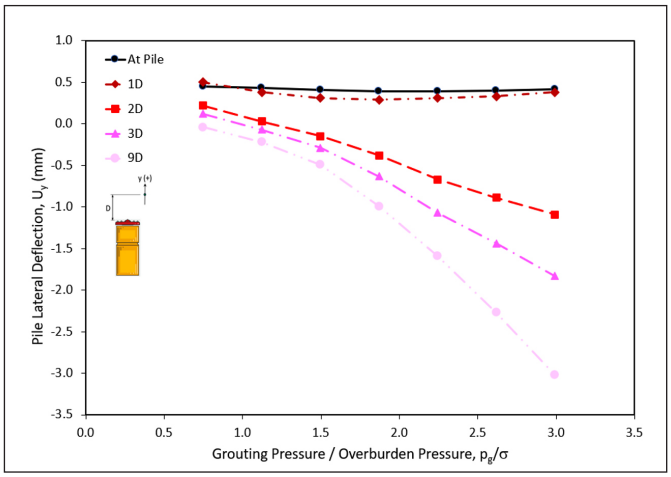

Figure 26: Pile lateral deflection, U_y vs. grouting pressure/overburden pressure, p_g/σ

4.2.3 Pile Axial Load

Figure 27 offers insights into the development and distribution of pile axial load during the TBM passage under varying applied grouting pressures. Additionally, Figure 28 presents the maximum axial load (compression) experienced by the pile in response to the effects of grouting pressure. As anticipated, downdrag load resulting from negative skin friction, caused by

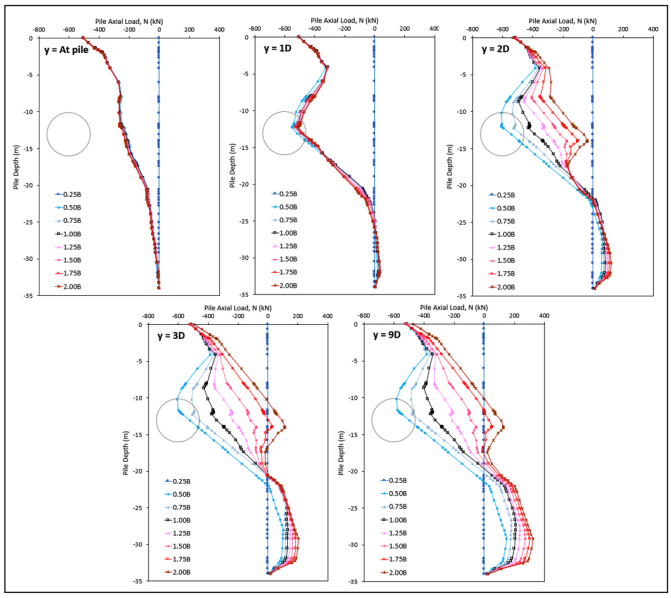

Figure 27: Development and distribution of pile axial load

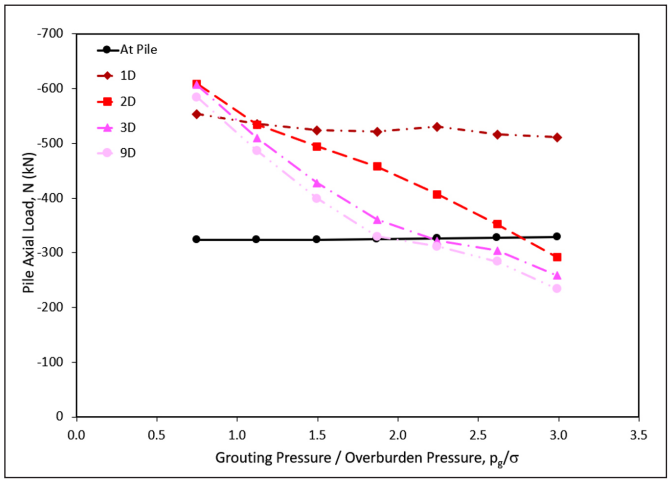

Figure 28: Pile axial load vs. grouting pressure/overburden pressure, p_g/σ

tunnelling-induced ground settlement, is generated. The pile demonstrates responsiveness to this, influence when the TBM is positioned at y = 2D and beyond.

The primary observation suggests that higher grouting pressure induces ground heaving, including pile head heaving, as depicted in Figure 24. This effect proves advantageous in swiftly counteracting negative skin friction quickly. It is plausible that the resulting additional positive skin friction contributes to enhancing the geotechnical capacity of the pile. Conversely, lower grouting pressure (p_g/σ < 1.0) leads to increased downdrag load compared to the baseline scenario.

4.2.4 Ground Surface Settlement

Figure 29 illustrates the overall trend of maximum ground settlement and ground loss within the range of p_g/σ ratio considered in this study. Notably, the recommended optimum grouting pressure is identified between 1.1 to 1.5 times the overburden pressure. This range correlates with the lowest magnitudes of ground settlement and ground loss, demonstrating its effectiveness in minimising the impact on the

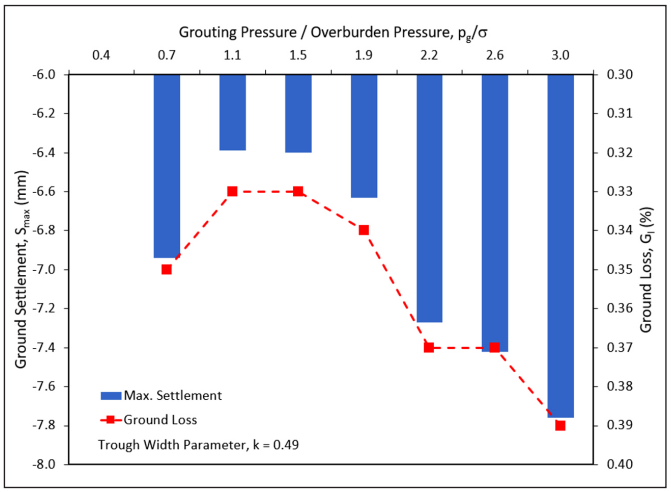

Figure 29: Ground settlement vs. grouting pressure/overburden pressure, p_g/σ

adjacent pile and surrounding ground. It is crucial, however, to consider the implications of applying higher grouting pressure in the design of the tunnel lining design.

4.0 CONCLUSIONS

This study conducted a comprehensive numerical investigation to evaluate the effects of varying face support pressures and tail skin grouting pressures on tunnelling-induced pile responses and ground surface settlement. The three-dimensional finite element model, calibrated and validated using field measurements and tunnelling data from a full-scale field research study, provided valuable insights into tunnel-soil-pile interactions.

The parametric analysis revealed distinctions tunnelling behaviours, particularly between negative face loss - occurring when normalised face pressure exceeds 1.0 - and positive face loss, when face pressure falls within or below the overburden pressure. This distinction highlights the critical influence of both face support and tail skin grouting pressures on pile responses and ground settlement during tunnelling operations.

Significant patterns in pile displacements were observed, notably in pile head settlement and lateral deflections, which varied across different tunnel excavation stages. The study also examined pile axial load distribution and ground settlement within the critical tunnel influence zone. The findings emphasise the importance of maintaining adequate face support pressures to mitigate excessive ground settlements and pile deformations. An optimum face support pressure range of 0.8 to 1.1 times the overburden pressure was identified, minimising pile responses and ground settlement.

Regarding tail skin grouting pressure, increasing grouting pressure was found to reduce pile head settlement while inducing exponential transverse lateral deflections and longitudinal pile rotation. Axial force analyses suggested that higher grouting pressure could induce ground heaving, counteracting negative skin friction and resulting in reduced axial loads. An optimum grouting pressure range of 1.1 to 1.5 times the overburden pressure was recommended to minimise ground loss and settlement, although the potential implications on tunnel lining design warrant careful consideration.

This research highlights the capability of advanced numerical models in capturing the complexities of shield tunnelling processes, non-linear soil-structure interactions, and transient tunnelling effects beyond conventional methods. The validated numerical framework provides a robust basis for further parametric studies to optimise tunnelling parameters and mitigate adverse impacts on adjacent piles, paving the way for more resilient tunnel design and construction practices.

ACKNOWLEDGEMENTS

The authors extend their gratitude to the management of Mass Rapid Transit Corporation Sdn. Bhd. for granting permission to publish this paper and for their positive support, which significantly contributed to the success of this work. Special thanks are also extended to Ir. Dr. Ooi Lean Hock of MMC-Gamuda KVMRT (T) Sdn. Bhd. for his insightful suggestions and guidance, without which the full-scale field measurement would not have been possible. The support rendered by Dr Tee Bun Pin of Smart Sensing Technology Sdn. Bhd. in the installation of the in-pile instrumentation, including fibre optic cables and vibrating wire strain gauges, is highly appreciated.

AUTHORS' CONTRIBUTIONS

- **Chee Min Khoo:** Data collection, methodology, analysis, interpretation, writing.
- **Hisham Mohamad:** Conceptualisation, study design, and supervision. ■

REFERENCES

[1] [1] Cham, W. M. (2007). *The response of piles to tunnelling*. MSc thesis, Imperial College, London.

[2] Couts, D. R., & Wang, J. (2000). Monitoring of reinforced concrete piles under horizontal and vertical loads due to tunnelling. In J. Zhao, N. Shirlaw, & R. Khrisnan (Eds.), *Tunnels and Underground Structures* (pp. 541-546).

[3] Herrenknecht, M., & Rehm, U. (2003). *Earth pressure balanced shield technology*. Internal lecture in colorado school of mine, USA.

[4] Jacobsz, S. W., Bowers, K. H., Moss, N. A., & Zanardo, G. (2005). The effects of tunnelling on piled structures on the CTRL. In *5th International Symposium on Geotechnical Aspects of Underground Construction in Soft Ground*, June 15-17, 2005, Amsterdam, Netherlands.

[5] Kaalberg, F. J., Teunissen, E. A. H., van Tol, A. F., & Bosch, J. W. (2005). Dutch research on the impact of shield tunnelling on pile foundations. In *5th International Symposium on Geotechnical Aspects of Underground Construction in Soft Ground,* June 15-17, 2005, Amsterdam, Netherlands.

[6] Kasper, T., & Meschke, G. (2004). A 3D finite element simulation model for TBM tunnelling in soft ground. *International Journal for Numerical and Analytical Methods in Geomechanics*, 28(14). 1441-1460.

[7] Khoo, C. M. (2024). *The transient effects of shield tunnelling on a loaded pile*. PhD thesis, Universiti Teknologi PETRONAS.

[8] Khoo, C. M., Mohamad, H., Tee, B. P., & Ghazali, M. F. (2024a). Field measurement of pile transient lateral response to advancing tunnel. *In Proceedings of ITA-AITES World Tunnel Congress (WTC 2020)*, April 25-29, 2024, Shenzhen, China.

[9] Khoo, C. M., Mohamad, H., Beddelee, A. A. A. M., Thansirichaisree, P., Ghazali, M. F., & Mohd Nasir, M. Y. (2024b), Effects of advancing tunnel on a loaded pile: numerical analysis and field measurements. *Journal of Rock Mechanics and Geotechnical Engineering*. In Press.

[10] Khoo, C. M., Mohamad, H., Mohd Nasir, M. Y., & Thansirichaisree, P. (2024c). Some insights into three-dimensional modelling of tunnel excavation. *International Journal of GEOMATE*. 27(120).

[11] Klar, A., Bennett, P. J., & Soga, K. (2006). Distributed strain measurement for pile foundations. In *Proceedings of the Institution of Civil Engineers, Geotechnical Engineering,* 159(3), 135-144.

[12] Lee, R. G., Turner, A. J., & Whitworth, L. J. (1994). Deformations caused by tunnelling beneath a piled structure. *In XIII ICSMFE*, New Delhi, India (pp. 873-878).

[13] Loganathan, N. (2016). Design charts: tunnelling-induced effects on adjacent pile foundation. In *Proceedings of 19th Southeast Asian Geotechnical Conference & 2nd AGSSEA Conference,* Kuala Lumpur, Malaysia (pp. 1125-1130).

[14] Mair, R. J. (1993). Unwin Memorial Lecture – Developments in geotechnical engineering research: application to tunnels and deep excavations. In *Proceedings of the Institution of Civil Engineers, Civil Engineering*, 97(1), 27-41.

[15] Mohamad, H., Soga, K., & Bennett P. J. (2009). Fibre optic installation techniques for pile instrumentation. In *Proceedings of the 17th International Conference on Soil Mechanics and Geotechnical Engineering: The Academia and Practice of Geotechnical Engineering*, IOS Press, 3, pp. 1873-1876.

[16] Mohamad, H., Bennett, P. J., Soga, K., Mair, R. J., & Bowers, K. (2010). Behaviour of an old masonry tunnel due to tunnelling-induced ground settlement. *Géotechnique*, 60(12), 927-938.

[17] Mohamad, H., Soga, K., Pellew, A., & Bennett, P. J. (2011). Performance monitoring of a secant piled wall using distributed fibre optic strain sensing. *Journal of Geotechnical and Geoenvironmental Engineering*, 137(12), 1236-1243.

[18] Mohamad, H, Soga, K., Bennet, P. J., Mair, R. J., & Lim, C. S. (2012). Monitoring twin tunnel interaction using distributed optical fibre strain measurements. *Journal of Geotechnical and Geoenvironmental Engineering*, 138, 957-967.

[19] Mohamad, H., Tee, B. P., Ang, K. A., & Chong, M. F. (2016). Characterizing anomalies in distributed strain measurements of cast-in-situ bored piles. *Jurnal Teknologi*, 78(8-5), 75-82.

[20] Mohamad, W., Bourgeois, E., Kouby, A. L., Szymkiewicz, F., Michalski, A., Branque, D., Berthoz, N., Soyez, L., Kreziak, C. (2022). Full scale study of pile response to EPBS tunnelling on a Grand Paris Express site. *Tunnelling and Underground Space Technology,* 124, 104492.

[21] Mollon, G., Dias, D., & Soubra, A. (2013). Probabilistic analyses of tunnelling-induced ground movements. *Acta Geotechnica,* 8. 181-199.

[22] Ohno, H., Naruse, H., Kurashima, T., & Nobiki, A. (2002). Application of Brillouin scattering-based distributed optical fibre strain sensor to actual concrete piles. *IEICE Transaction on Electronics E85*, 945-951.

[23] Pang, C. H., Yong, K. Y., Chow, Y. K., & Wang, J. (2005). Response of pile foundation subjected to shield tunnelling. In *5th International Symposium on Geotechnical Aspects of Underground Construction*, June 15-17, 2005, Amsterdam, Netherlands.

[24] Selemetas, D, Standing, R. J., & Mair, R. J. (2005). The response of full-scale piles to tunnelling. In *5th International Symposium on Geotechnical Aspects of Underground Construction in Soft Ground*, June 15-17, 2005, Amsterdam, Netherlands.

[25] Soga, K., Mohamad, H., & Bennett, P. J. (2008). Distributed fibre optics strain measurements for monitoring geotechnical structures. In *6th International Conference on Case Histories in Geotechnical Engineering* (Symposium in honour of Professor James K Mitchell), Arlington, USA.

[26] Tan, Y. C., Teh, W. S., & Gue, C. S. (2019). Special design considerations for underpinning system for existing structures due to tunnelling. In *Proceedings of ITA-AITES World Tunnel Congress* (WTC 2019), Naples, Italy.

[27] Tee, B. P., Mohamad, H., Ang, K. A., & Chong, M.F. (2016). Load test performance of bored pile with distributed fibre optic strain sensing. In *Proceedings of 19th Southeast Asian Geotechnical Conference & 2nd AGSSEA Conference,* Kuala Lumpur, Malaysia (pp. 865-870).

[28] Tee, B. P., Rashid, A. S. A., Abdullah, R. A., Kassim, K. A., & Mohamad, H. (2017). Application of distributed fibre optic sensor in instrumented pile load test. *Asean Engineering Journal.*

[29] Teunissen, E. A. H., & Hutteman, M. (1998). Pile and surface settlement at full scale tests North/South Line metro. In *Proceedings of the World Tunnel Congress'98*, São Paulo, Brazil.

[30] Vermeer, P. A., Bonnier, P. G., & Möller, S. C. (2002). On a smart use of 3D-FEM in tunnelling. *Proceeding of 8th International Symposium on Num. Models in Geomech–NUMOGVIII*, 361–366. Balkema, Rotterdam.

PROFILES

CHEE MIN KHOO holds a Bachelor's degree with First Class Honours from Universiti Teknologi Malaysia and both an MSc degree and PhD in Civil Engineering from Universiti Teknologi PETRONAS. With over 20 years of extensive experience, he is a recognised specialist in geotechnical and tunnel engineering, with expertise in consultancy and design management. He has published nearly 40 technical papers and received the prestigious Tan Sri Hj. Yusoff Prize in 2019, the highest recognition for outstanding civil engineering papers by corporate members of IEM.
Email address: khoocheemin@gmail.com

HISHAM MOHAMAD is the Chair of Civil & Environmental Engineering Department, Universiti Teknologi PETRONAS. He is the leading expert in Distributed Fibre Optic Sensing (DFOS) for infrastructure and structural health monitoring. His invention, Smart Geopipe (TRL-8) received multiple recognitions and as best innovative product by national and international bodies, including invited to showcase at the United Nations' COP28. At UTP, he founded Smart Infrastructure Modelling & Monitoring research centre and responsible for securing and managing multi-million ringgit industrial and consultancy projects.
Email address: hisham.mohamad@utp.edu.my